Journal of Building Engineering 40 (2021) 102761

Contents lists available at ScienceDirect

Journal of Building Engineering

journal homepage: http://www.elsevier.com/locate/jobe

Geopolymers made from metakaolin sources, partially replaced by Spanish clays and biomass bottom ash

D. Eliche-Quesada [a, b, *], A. Calero-Rodríguez [a], E. Bonet-Martínez [a], L. Pérez-Villarejo [a, b], P.J. Sánchez-Soto [c]

[a] Department of Chemical, Environmental and Materials Engineering, Higher Polytechnic School of Jaén, University of Jaén, Campus Las Lagunillas, S/n, 23071, Jaén, Spain
[b] Center for Advanced Studies in Earth Sciences, Energy and Environment (CEACTEMA), University of Jaén, Campus Las Lagunillas, S/n, 23071, Jaén, Spain
[c] Materials Science Institute of Sevilla (ICMS), Joint Center Spanish National Research Council (CSIC)-University of Sevilla, C/Américo Vespucio, 49, 41092, Sevilla, Spain

ARTICLE INFO

Keywords:
Biomass bottom ash
Spanish clays
Geopolymers
Mechanical properties
Sustainability

ABSTRACT

The main objective of this investigation is to study the effect of the substitution of metakaolin (MK) (from calcined industrial kaolin) by four different calcined natural Southern Spain clays traditionally used in the brick and tile sector, as well as by the biomass bottom ash residue (BBA) from the combustion of a mix of olive and pine pruning on the synthesis of geopolymer with physical, mechanical and thermal properties comparable to those of classic construction materials. As alkaline activator, a 8 M solution of sodium hydroxide and sodium silicate have been used. Raw materials, metakaolin; Spanish clays: black clay (BC), yellow clay (YC), white clay (WC), red clay (RC) and BBA were characterized by chemical analysis (XRF), mineralogical analysis (XRD), and particle size analysis. Control geopolymers containing only metakaolin, and batch of geopolymers were formulated containing equal proportions of metakaolin, BBA and each of the four types of clay. After the curing period, at 60 °C for 1 day geopolymers were demolded and stored 27 days at room temperature. Geopolymers were characterized using Scanning Electron Microscopy coupled with Energy Dispersive Spectroscopy (SEM-EDS), XRD and Attenuated Total Reflectance- Fourier Transform Infrared Spectroscopy (ATR-FTIR). Their physical, mechanical and thermal properties have also been studied. The addition of BBA and different types of calcined clays to metakaolin gives rise to geopolymers with higher mechanical properties increasing the compressive strength of the control geopolymer containing only MK (24.9 MPa) by more than 50% for the GMK-BBA-WC geopolymers (38.5 MPa). The clays act as fillers and/or promote the precipitation of calcium-rich phases (Ca)-A-S-H-G gel that coexists with the (Na)-A-S-H gel type. The relevant results of physical, mechanical and thermal properties obtained in this research demonstrate the potential of Spanish clays and BBA as binders and substitutes for metakaolin.

1. Introduction

The development of alternative cementitious products to Portland cement (PC), through processes that involve lower emissions of polluting gases into the atmosphere and with an appreciable energy improvement, is a priority line of research worldwide. The cement industry has developed alternative cementitious materials, such as cement additives and alkaline activated cements or geopolymers. In cement-based materials it has been possible to reduce the amount of clinker, through its partial replacement by chemically active additions such as pozzolans and industrial by-products (metallurgical slags and coal ash) [1]. The geopolymers or alkali activated cements are the most promising cements, besides being more eco-efficient materials, due to their low environmental impact. Geopolymerization is a chemical reaction between a aluminosilicate source and an alkaline activator, such as caustic alkalis or alkaline salts. Thus, in order to carry out the development of these new materials, a strongly alkaline dissolution is required, such as sodium or potassium hydroxides and sodium or potassium silicates, which raise the pH of the medium. The reactive materials of the aluminosilicate type dissolve in an alkaline medium and form oligomers, $Si(OH)_4$- and $Al(OH)_4$- and hydroxylated compounds during the polycondensation reaction. The tetrahedral units are alternately joined to form an amorphous network that constitutes the geopolymers [2,3]. The alkaline activated materials or geopolymers are considered the ma-

* Corresponding author. Department of Chemical, Environmental and Materials Engineering, Higher Polytechnic School of Jaén, University of Jaén, Campus Las Lagunillas, s/n, 23071, Jaén, Spain.
E-mail address: deliche@ujaen.es (D. Eliche-Quesada).

https://doi.org/10.1016/j.jobe.2021.102761
Received 23 January 2021; Received in revised form 2 May 2021; Accepted 17 May 2021
Available online 23 May 2021

terials of the future due to their low environmental impact by considerably reducing CO_2 emissions and presenting low energy consumption and high performance relative to the consumption of raw materials [4]. Consequently, one of the strategies to fight climate change is the production of materials with less environmental impact. This fact can contribute to a more sustainable and eco-efficient future "revolution" in the sector of building materials (cement, concrete and ceramics) with structural capacity.

Spain is one of the countries with large deposits of clays. Spanish clays until now have been mainly used in the traditional ceramic industry [5,6]. However, currently Spanish clays are being used in more innovative applications such as pozzolanic material [7], material for the retention of two widely used non-ionic fungicides, metalaxyl and fludioxonil [8], use in CO_2 capture processes [9], and pelotherapy [10]. An application of interest, scarcely studied, is the use of Spanish clays as a source of aluminosilicate for the synthesis of alkaline activated materials or geopolymers. Its use as a source of aluminosilicates can be a profitable potential application reducing the cost of raw materials In most of the studies the clays were calcined at different temperatures and times [11–15]. The calcination process transforms the non-reactive crystalline phases into reactive amorphous phases. Often the fresh geopolymers prepared with these calcined clays are cured at elevated temperatures since a thermal treatment can that lead to an improvement of the strength of the geopolymers [16,17].

On the other hand, in order to reduce CO_2 emissions, the International Energy. Agency indicates that the current trend is to increase the use of renewable energy as substitutes for fossil fuel energy. According to the European Directive 2009/28/EC [18], the amount of renewable energy consumed in the coming years should be increased. This has caused the number of renewable energy plants in Spain to increase. Andalusia region is the first one in the ranking of the sector of electricity generation using biomass, with 17 installations totaling 273.98 MW, due to the significant potential of olive cultivation and associated industries. In recent years, the energy generated from energy crops, such as pines, poplars and especially eucalyptus, has grown significantly [19].

The generation of energy from the combustion of biomass generates as wastes biomass fly ash (BFA) and biomass bottom ash (BBA). Both residues are formed by unburned particles in the combustion process. BFAs have been more widely used as fertilizer in agriculture [20]. However, both BFA and BBA are suitable for soil application as well as for incorporation on road or cementitious materials [21–23]. Although the use of BFA has been extensively investigated, studies on the use of BBA have been minors. BBAs are normally deposited in landfills. Despite the high production of BBA in Spain, 43,200 t/year [24], most of them have no application and are deposited in landfills. BBA meet the requirement of geopolymer binder, with a considerable amount of silica and alumina. The effect of BBA on the properties of metakaolin geopolymers was studied [25]. However, no studies have been conducted in which metakaolin has been partially replaced by different Spanish calcined clays and biomass bottom ash. Therefore, the study of the properties of geopolymers containing metakaolin, BBA and different types of Spanish calcined clays, will provide significant data on the influence of the type of clay and the incorporation of BBA on the physical, mechanical and thermal behavior of geopolymers. The knowledge of the properties of the new geopolymers that incorporate BBA and calcined clays will allow define new ways of applying BBA waste; and the raw materials available in the area, will allow a sustainable use of by-products and natural resources in the construction sector to go towards a circular economy. This is the main aim of the present study.

2. Materials and methods

2.1. Raw materials and characterization of raw materials

The raw materials used as a source of aluminosilicates in the production of geopolymers were: metakaolin (MK), four different Spanish clays and biomass bottom ashes (BBA). The metakaolin was obtained by calcination at 750 °C for 4 h of the kaolin supplied by the company Caobar S.A. located in Guadalajara (Spain). Clays have been extracted from quarries located in the province of Jaén (Spain) and they have been supplied by Arcillas Bailén (Jaén, Spain). Black, yellow and red clays are used as raw material in the production of bricks and ceramic tiles, while white clays are used for ornamentation. These raw materials are dark gray marls (black clay, BC), yellowish loamy clays with some intercalations of silt and sand (yellow clay, YC), light gray clayey loam (white clay, WC) [26] and clays belonging to the Red Layers of Tabular Coverage (red clay, RC) [26]. Therefore, the clays used in this research have been coded according to their colour (B = black; Y = yellow; W = white; R = red). The clays were crushed and ground to produce a powder with a particle size suitable to pass through a 150 μm sieve. The clays were activated by calcination at 750 °C for 4 h. Thermogravimetric -thermodifferential analysis (TGA-DTA) of kaolin and clays was used to determine the temperature and time of the heat treatment [27,28] (Fig. 1). At 550 °C, dehydroxylation of kaolinite takes place with the formation of metakaolinite [27] (Fig. 1a). The behavior of the four Spanish clays is similar. The dehydroxylation of the silicates present in the clays takes place between 400 and 600 °C and the decomposition of carbonates between 700 and 740 °C (Fig. 1b–e). Therefore, a temperature of 750 °C was selected according to previous results [25,29–31]. Biomass bottom ashes (BBA) were supplied by the plant Aldebarán Energía located in Ándujar (Jaén, Spain). This industry generates renewable energy from biomass from olive tree pruning, forest biomass and energy crops. The ashes were conditioned by grinding and sieving until a particle size of less than 150 μm was obtained.

The particle size distribution of the raw materials was analyzed using the Malvern Mastersizer 2000LF Particle Size Analyzer (Malvern Instruments Ltd). The particle size distribution of the calcined clays (MK, YC, BC, WC, RC) and the biomass bottom ash (BBA) is shown in Fig. 2. The average particle size (D_{50}) of the four clays ranges from 25.2 to 39.9 μm for RC and BC, respectively. The average particle size of bottom ash is 52.6 μm upper to metakaolin being the finest with D_{50} = 9.6 μm.

The main fraction of calcined clays is made up of silt-size particles (2–63 μm), while BBA are mainly made up of sand-sized particles (63–2000 μm) (Table 1).

An AccuPyc II 1340 pycnometer with helium was used to measure the true density of the raw materials. The true density for MK is 2630 kg/m^3. Calcined clays are denser, with true densities of 2721, 2722, 2781 and 2789 kg/m^3 for RC, YC, WC and BC, respectively. Biomass bottom ash is slightly lighter wih a true density of 2546 kg/m^3.

The chemical composition of the raw materials used as a source of aluminosilicates has been determined by the X-ray fluorescence (XRF) technique using a Philips Magix Pro model PW-2440 X-ray fluorescence equipment. MK is mainly composed of SiO_2 (58.03 wt %) and Al_2O_3 (40.29 wt %). Calcined clays and BBA have a high content of SiO_2, presenting high amounts of Al_2O_3 but less than MK (Table 2). They also present considerable amounts of other elements such as CaO (WC, YC, BC and BBA), Fe_2O_3 (RC), MgO and K_2O. Due to the high calcium content of calcined clays (WC, YC and BC) and BBA, it is expected that in the geopolymers prepared using these raw materials, together with geopolymeric gel, calcium silicate gel (CSH) will form within the hydration products [15].

The crystalline phases present in the raw materials and the geopolymers were evaluated by X-ray diffraction (XRD) using an Empyrean equipment with a PIXcel-3D detector from PANalytical. Cu Kα radiation

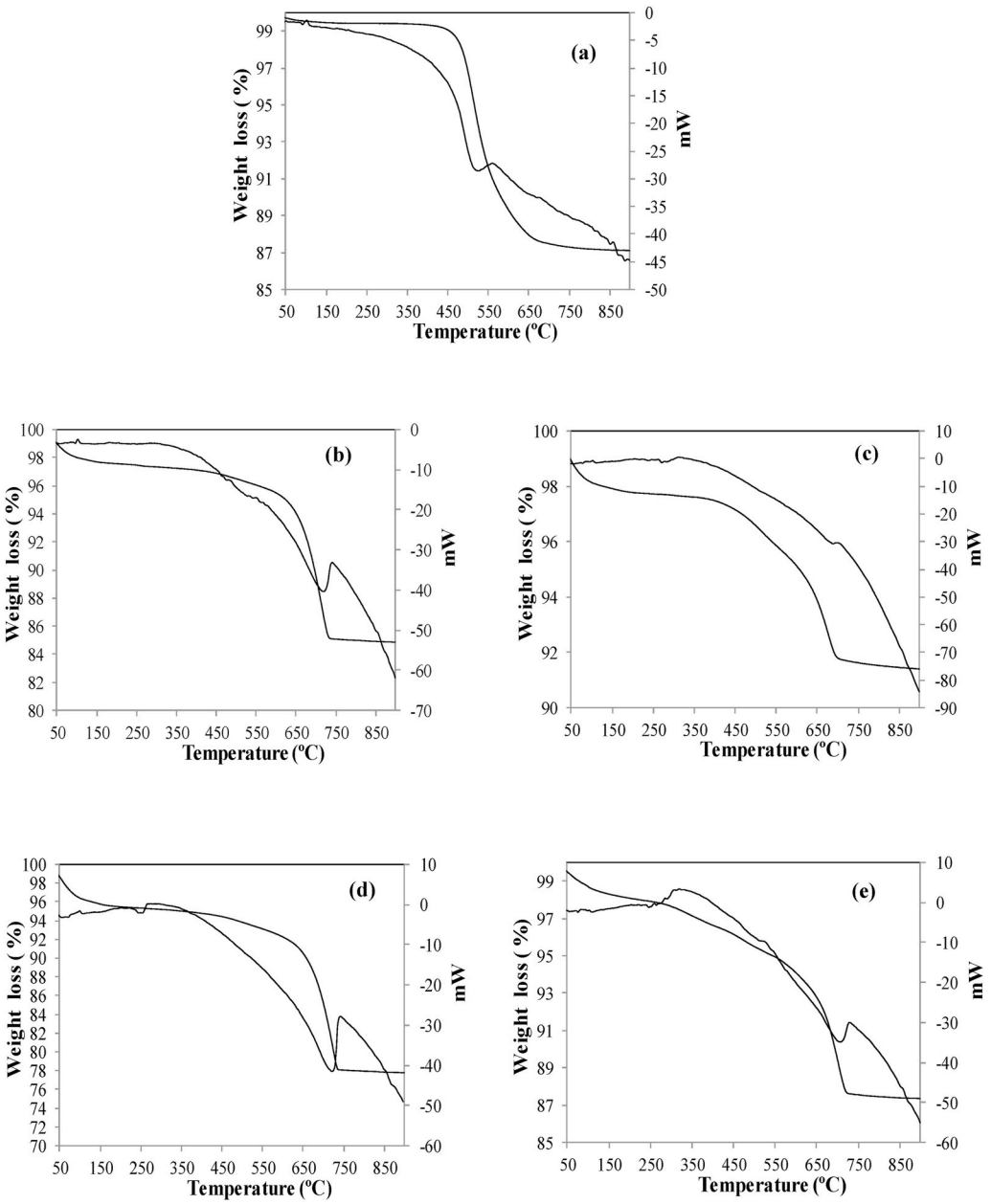

Fig. 1. TGA-TDA of raw materials:(a) caolin; (b) raw yellow clay; (c) raw red clay; (d) raw white clay and (e) raw black clay.

(λ = 1.5406 Å) has been used at 40 kV and 40 mA, in a 2 θ range from 10 to 60° and a step size of 0.02°. The percentage of amorphous phase of the raw materials and of the geopolymers after 28 days of curing was determined with the Ohlberg method [32]. Silicon dioxide (Carlo Erba RPE, Cas 14808-60-7) was used as a standard to characterize the amorphous phase. The HighScore software (versión 4.7, Malvern PaNalytical) was used to identify the phases and perform the semi-quantitative analysis. Fig. 3a shows the XRD pattern of kaolin after the 750 °C firing process. Quartz is observed as the main crystalline phase, not showing the diffraction peaks of kaolinite. This fact indicates that kaolin is transformed in metakaolin accompanied by a hump in the 2θ region between 20 and 30° associated to the presence of an amorphous phase [33] (Table 3).

After the heat treatment at 750 °C, Table 3 and Fig. 3b show the mineralogy of the raw materials. The BC, RC and YC calcined clays show quartz and illite as main crystalline mineralogical species. The RC also shows to a lesser extent muscovite and the YC and the BC the feldspar orthoclase. The WC has quartz and orthoclase as main crystalline phases. The percentage of amorophous materials from XRD measurements indicated that MK is higher (90%) with variable contents in the range 27.4–57.5 for the calcined clays (Table 3).

The diffraction pattern of BBA (Table 3, Fig. 3c) indicates that the waste is mainly composed of silica, and to a lesser extent by calcium carbonate, also presenting some aluminosilicates and lime in lower proportion.

2.2. Geopolymers preparation and characterization

An alkaline activator solution with silica modulus (R = SiO_2/Na_2O) of 0.73 was prepared by dissolving sodium silicate solution in an 8 M solution of sodium hydroxide. Sodium hydroxide (NaOH) has been used in pellets with a purity of 98%. An 8 M solution of sodium hydroxide has been used. Sodium silicate has a density of 1365 kg/m^3 and a composition of: H_2O (61.9 wt %), SiO_2 (29.2 wt %) and Na_2O (8.9 wt %). Both reagents have been provided by the company Panreac S.A.The activating solution has a pH of 13.3.

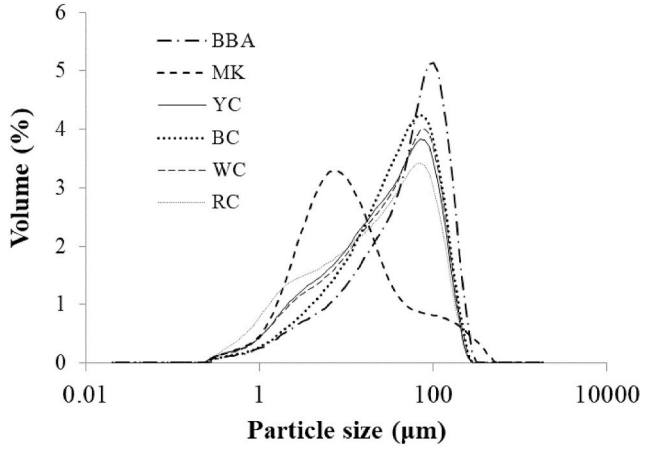

Fig. 2. Particle size distribution of raw materials.

Table 1
Particle size distribution of calcined clays (MK, BC, WC, YC, RC) and BBA.).

Particle size (μm)	MK (%)	BBA (%)	YC (%)	RC (%)	WC (%)	BC (%)
Clay (< 2)	8.13	15.25	4.64	7.69	4.50	2.92
Silt (2–63)	78.98	33.25	57.82	59.06	55.72	54.58
Sand (63–2000)	12.89	51.51	37.53	33.25	39.76	42.50

Table 2
Chemical composition of raw materials, metakaolin (MK), biomass bottom ash (BBA) and the calcined clays: black clay (BC), white clay (WC), yellow clay (YC) and red clay (RC).

Compound	MK	BBA	RC	YC	BC	WC
SiO_2	58.03	46.10	55.70	48.08	51.82	48.49
Al_2O_3	40.29	12.04	21.19	12.77	14.90	12.76
Fe_2O_3	0.42	4.78	8.05	4.69	4.95	4.75
MnO	0.01	0.09	0.09	0.06	0.02	0.06
MgO	0.11	3.71	2.94	3.16	2.01	3.16
CaO	0.09	19.65	3.01	23.60	13.68	23.78
Na_2O	0.02	0.78	0.37	0.41	0.80	0.41
K_2O	0.39	4.59	5.77	2.23	2.89	2.21
TiO_2	0.15	0.83	0.93	0.67	0.84	0.66
P_2O_5	0.07	1.12	0.15	0.15	0.13	0.15
SO_3	0.01	0.41	0.07	0.13	5.53	0.05
LOI	0.36	5.58	1.49	3.69	2.20	3.11

The preparation of the fresh mixture was done by mixing MK, a type of calcined clay and BBA with the alkaline solution. Geopolymers present the same amounts of the three raw materials, therefore the amount of substitution of MK for calcined clays was 33.33 wt % and another 33.33 wt % for BBA. A composition with 100 wt % of MK was prepared as reference. After a preliminary investigation, the water/binder ratio remained constant and equal to 0.6 to obtain adequate plasticity of the mixture. The binder is calculated as the sum of all solid precursors, the anhydrous activator, NaOH, and solid contained in the sodium silicate solution. Details on the proportion of the mixtures are presented in Table 4.

The raw materials were homogenized: MK, calcined clays and BBA in a dry state for 5 min in a Proeti planetary mixer. The alkaline activator is then added and mixed for 2 min at low speed. Finally, the geopolymeric precursor was homogenized for 10 min, at fast speed of the mixer until obtaining a homogeneous paste. The mixture is then poured into 25 mm diameter polyethylene molds up to a height of about 50 mm. The molds were vibrated on a shaking table during 2 min to eliminate air bubbles. The specimens were cured at 60 °C and a saturated atmosphere for 24 h. After this period, the samples are removed from the mold and kept at room temperature until the age of the test, 28 days. (Fig. 4). The amount of carbonates has been determined by calcimetry [34]. To dissolve the aluminosilicate gels formed, the HCl extraction method was used [35]. For the extraction with HCl, 1 g of ground and sieved geopolymer (150 μm) was attacked with a 250 ml solution of HCl (1:20) for 3 h. Subsequently the solution was filtered and the insoluble residue was washed with deionized water and dried to constant weight. The percentage of weight loss was determined by weighing the insoluble residue.

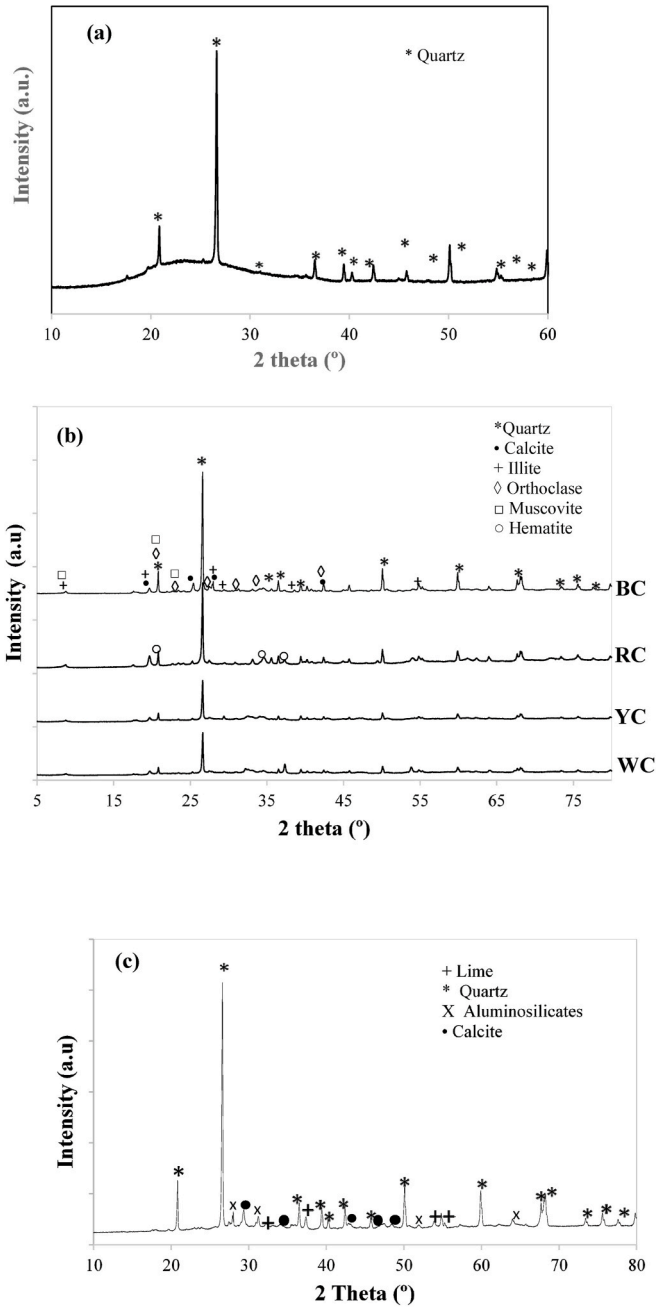

Fig. 3. XRD pattens of raw materials: (a) metakaolin (MK); (b) red clay (RC), yellow clay (YC), black clay (BC) and white clay (WC) and (c) biomass bottom ash (BBA).

The bulk density was determined by the Archimedes method with inmersion technique in accordance with the UNE-EN 1015-10 standard [36]. Three geopolymer samples of each composition 25 mm in diameter and approximately 50 mm in height were immersed in water and the bulk density (ρ) and apparent porosity were calculated according to the equations:

Table 3
Mineralogical composition of raw materials (thermal treatment at 750 °C/4 h MK and different calcined clays).

Raw materials	Amorphous (wt %)	Major Component	Minor component	Traces
MK	90.0	Quartz	–	–
BBA	24.5	Quartz	Calcite, aluminosilicates, lime	–
RC	57.5	Illite, quartz, muscovite	Hematite	Orthoclase
YC	27.4	Quartz, illite, orthoclase	Lime, hematite	Calcite
BC	32.1	Quartz, illite, orthoclase	Hematite	Lime, calcite
WC	27.7	Quartz, orthoclase	Lime, montmorillonite, hematite	Muscovite, calcite

Table 4
Formulation of geopolymer samples and Si/Al and Na/Si molar ratio. Clay indicates RC, YC, BC or WC clays.

Sample	MK (g)	Clay (g)	BBA (g)	Na_2SiO_3 solution (g)	H_2O[a] (g)	NaOH (g)	Si/Al Molar Ratio	Na/Si Molar Ratio	Ca/(Si + Al) Molar Ratio
GMK	450	–	–	300	195	64	1.68	0.7	0.0008
GMK-RC-BBA	150	150	150	300	195	64	1.98	0.7	0.09
GMK-YC-BBA	150	150	150	300	195	64	2.17	0.7	0.18
GMK-BC-BBA	150	150	150	300	195	64	2.11	0.7	0.14
GMK-WC-BBA	150	150	150	300	195	64	2.15	0.7	0.19

[a] Water from the 8 M NaOH solution. Water from the sodium silicate solution (185.7 g) is not included.

Fig. 4. Geopolymers samples: GMK; GMK-YC-BBA; GMK-RC-BBA; GMK-WC-BBA; GMK-BC-BBA.

$$\rho = \frac{md}{ma - mw}\rho_w \quad (1)$$

$$Pa = \frac{ma - md}{ma - mw} * 100 \quad (2)$$

where m_d is dry mass, m_a is the mass of the saturated samples in air, m_w is mass of the saturated samples in water and ρ_w is the density of water 1000 kg/m^3.

Water absorption (W_a) was determined using the equation:

$$W_a \frac{ma - ms}{ms} * 100 \quad (3)$$

A MTS 810 Material Testing Systems laboratory of 100 kN with a displacement rate of 0.5 mm/min was used to perform the mechanical tests for compressive strength (Cs) of six geopolymers (25 mm diameter; 50 mm height) according to the standard procedure UNE-EN-772-1 [37] and calculated using the following equation:

$$Cs = \frac{P}{A} \quad (4)$$

where P is the maximum force and A is the unit of area over which it acts.

Thermal properties of the geopolymers were determined at 10 °C according to ISO 8302 standard [38] using the FOX 5-TA Instruments heat flow meter. Two samples of 55 mm in diameter and 15 mm in height were used.

Geopolymer microstructures were examined using a JEOL SM 840 model scanning electron microscope (SEM) coupled by Energy dispersive X-ray Spectroscopy (EDS). Samples were coated with carbon using the JEOL JFC 1100 sputter coater. An Vertex 70 Bruker equipment of Attenuated Total Reflectance-Fourier Transform Infrared Spectroscopy (ATR-FTIR) was used for further analysis of the geopolymers in the range of 4000–400 cm^{-1} at room temperature.

3. Results and discussion

3.1. HCl extraction

The carbonate content (as wt. % of calcite in the sample) of raw sample and percentage of disolved mass after HCl extraction are presented in Table 5. The carbonates present in the raw materials dissolve in the HCl solution and an increase in the dissolved mass is observed as the carbonate content in the precursors increases. With respect to the geopolymers, a substantial increase in dissolved mass is observed in the geopolymer samples with respect to the precursors. This fact indicates the formation of sodium aluminosilicate hydrated and calcium aluminosilicate hydrated gels in all geopolymers [39,40]. Since the geopolymers have similar contents of carbonates due to the carbonation process with atmospheric CO_2 it can be concluded that in GMK and GMK-BBA-WC geopolymers present a higher amount of geopolymer gel.

3.2. Bulk density, apparent porosity and water absorption of geopolymers

The results of bulk density, apparent porosity and water absorption of the geopolymers after 28 days are shown in Table 6.

The bulk density of the control geopolymers was 1201 kg/m^3. The bulk density of metakaolin geopolymers is normally in the range between 1200 kg/m^3 and 1800 kg/m^3 [15]. Control geopolymers have a lower bulk density than those obtained by other authors [41]. Bulk density values were comparable to those obtained by Tippayasam et al. [42] for the metakaolin geopolymer obtained using 10 M potassium hydroxide after undergoing a 550 °C heat treatment. They found a value

Table 5
Carbonate content and results of the HCl extraction of the raw materials and geopolymers.

Sample	Carbonate content (wt%)	Mass dissolved by HCl (wt. %)
MK	4.00	28.01
BBA	11.53	74.21
YC	8.29	56.94
RC	5.07	31.44
WC	8.43	61.53
BC	6.31	56.10
GMK	7.06	79.76
GMK-BBA-RC	8.15	71.70
GMK-BBA-YC	8.90	65.80
GMK-BBA-BC	8.04	66.63
GMK-BBA-WC	8.34	78.32

Table 6
Bulk density, apparent porosity and water absorption of synthetized geopolymers.

Sample	Bulk density (kg/m^3)	Apparent porosity (%)	Water absorption (%)
GMK	1201 ± 16	53.0 ± 0.48	42.15 ± 0.93
GMK-BBA-RC	1272 ± 19	51.6 ± 0.65	41.85 ± 0.72
GMK-BBA-YC	1269 ± 16	49.0 ± 0.48	41.95 ± 0.72
GMK-BBA-BC	1270 ± 11	51.6 ± 0.65	41.64 ± 0.72
GMK-BBA-WC	1274 ± 6	51.4 ± 0.72	41.40 ± 0.43

of 1260 kg/m^3. Duxson et al. [43] indicated that metakaolin-based geopolymers with a Si/Al molar ratio <1.65 presented a porous microstructure, with larger pores (on the order of microns), than geopolymers with a Si/Al molar ratio >1.65 that are more homogeneous and contain pores smaller (on the order of nanometers). However, for the GMK control geopolymers synthesized in this research using MK, the Si/Al molar ratio = 1.68 was not enough to decrease accessible porosity. This suggested a decrease in the surface area of the gel due to capillary stress induced by shrinkage in the pore structure.

The replacement of 33.33% MK by BBA and another 33.33% by calcined clays gave rise to geopolymers with slightly higher bulk density (1269–1274 kg/m^3) than control geopolymers. The values of the bulk density were comparable with those obtained by other authors [44] for fly ash geopolymers (1180–1580 kg/m^3), decreasing the bulk density with the highest H_2O content in the paste. The use of BBA and clay to partially replace MK promoted a more compact structure formed by the filling and type gel enrichment effect. Regarding the influence of the type of clay added, it is observed that practically all the geopolymers present similar physical properties, due to the similarity in their true densities and mineralogical composition. This implies that the clay particles have a slightly higher pore-filling than MK, and there are no particles agglomeration effect [45]. The Si/Al molar ratio has no effect on the bulk density and apparent porosity of geopolymers, as other authors have indicated previously [46].

The porosity values of geopolymers fell in the range of 49.0–53.0% which were similares to those found by Longhi et al. [47], for metakaolin geopolymers (43.6–65.8%). The use of a high liquid content in the geopolymer mixture together with a less efficient activating solution to polycondensation resulted in the appearance of pores in the geopolymer matrix therefore, high porosity [48]. Finally, water absorption values of geopolymers synthesized using calcined clays are slightly lower than metakaolin geopolymers.

3.3. Mechanical properties of geopolymers

Mechanical properties are the most important index of engineering quality in ceramic materials for construction with structural functions. The mechanical strength of geopolymers is not only attributed to densification, but also to the cementitious products formed in the geopolymerization reaction.

Compressive strength data of geopolymers after 28 days showed that samples rupture does not occur suddenly, indicating ductile behaviour. This may be due to the minerals present in the calcined clays after heat treatment, especially the presence of illite, which provides to the geopolymers plasticity [49]. The compressive strenght result for the geopolymers is shown in Fig. 5. The control geopolymers (GMK), which was synthesized using only metakaolin, has a compressive strength of 24.9 MPa, being similar to that reported by other authors using similar Si/Al relationships [50]. The replacement of MK by BBA and by different types of Spanish calcined clays results in geopolymers with better properties of compressive strength with values between 26.8 (using YC) and 38.5 MPa (using WC). According to the bulk density data, these geopolymers have higher bulk density and lower water absorption and

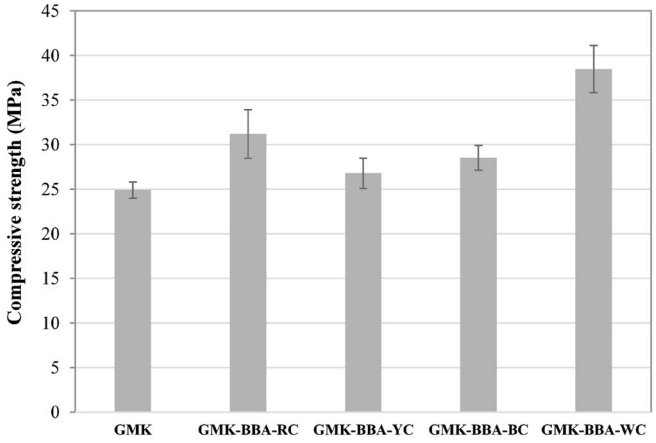

Fig. 5. Compressive strength of the geopolymers.

apparent porosity than the control geopolymers. Compressive strength follows the following increasing order GMK-BBA-YC < GMK-BBA-BC < MK-BBA-RC < MK-BBA-WC. Despite the lower metakaolinite content, the presence of minerals present in the calcined clays (illite, orthoclase, muscovite, hematite and quartz) can exert a reinforcement in these materials, acting as fillers [51]. It should be noted that MK-BBA-WC geopolymers presented the highest compressive strength (38.5 MPa), although the specimens present similar apparent porosity and bulk density as the rest of geopolymers (Table 6). There is a relationship between compressive strength and polycondensation in metakaolin geopolymers, which depends on the water/binder ratio, the chemical composition of the raw materials used and the activating solution. Polycondensation is favoured if the activating solution contains sodium silicate as the silicate species are already available in the solution. Consequently, the mechanical strength increases [52]. In the synthesis of geopolymers, both the water/binder ratio and the activating solution remain constant, so the factor to consider in compressive strength is the chemical composition. The increase in the Si/Al ratio causes the Si–*O*–Al bonds to decrease and the Si–*O*–Si bonds to increase in the gel geopolymer. Si–*O*–Si bonds are stronger by increasing mechanical strength of GMK- BBA-clay geopolymers with higher Si/Al molar ratio, and higher values of compressive strength are obtained.

Another factor to consider is the formation of calcium-rich phases that coexist with (Na)-A-S-H type gel, because the raw materials, BBA, WC, YC and BC are rich in CaO (Table 2). Other authors indicated that calcium rich sources can lead to the precipitation of a certain amount of C-(A)-S-H gel in combination with N-A-S-H gel. The formation of C-(A)-S-H gel can have a beneficial effect on the mechanical properties of the specimens [53,54]. GMK-BBA-WC geopolymers have the highest compressive strength and also the higher amount of calcium content. However, the calcium content of these geopolymers is similar to the calcium content of GMK-BBA-YC geopolymers (Table 2), indicating that the amount of geopolymer gel formed also has influenced in the compressive strength. The geopolymers using YC and BC as raw materials precursors (GMK-BBA-YC and GMK-BBA-BC) contain low amount of geopolymeric gel, according to HCl extraction (Table 5) and XRD data (Fig. 7a) and they have the lower mechanical properties (Fig. 5). Finally, an important aspect to consider in compressive strength is the presence of defects in specimens, such as micropores, microcracks and some spherical macropores. Microcracks can be propagated along the matrix and clearly visible on fracture surfaces, and distributed even in the defects in the specimens, such as micropores the matrix,. These defects are originated during the synthesis process due to the retention of air bubbles, as well as due to the contraction of evaporated water during drying step. This can be detected in the SEM micrographs (Fig. 11). Thus, these defects are larger in the GMK-BBA-YC and GMK-BBA-BC

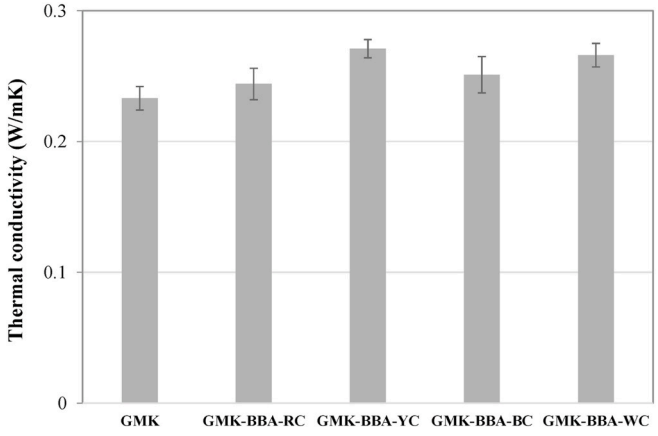

Fig. 6. Thermal conductivity of the geopolymers.

geopolymers. Pores act as stress concentration points and are prone to failure when the load is applied.

3.4. Thermal properties of geopolymers

The commitment made by society in relation to the energy efficiency required in all areas and particularly in construction, has led to the development of insulating materials that collaborate with the aim of improving the thermal behavior of new construction systems, and with adequate mechanical properties. One of the interests of the present research is to develop new modified geopolymers with good thermal insulation properties for buildings. The thermal conductivity data of the obtained geopolymers are presented Fig. 6.

Control geopolymers (GMK) have a thermal conductivity of 0.23 W/mK. These values are lower than those obtained by other authors. Kamseu et al. [55], obtained metakaolin-based geopolymers with thermal conductivities between 0.30 and 0.59 W/mK. Ain Jaya et al. [41], obtained metakaolin geopolymers with thermal conductivities in the range of 0.33–0.41 W/mK. However, the conductivity values obtained are similar to those obtained by these authors when they used 0.5% H_2O_2 as a foaming agent, because these geopolymers present similar values of bulk density and apparent porosity as the control geopolymers obtained in this work. Pore formation reduces thermal conductivity due to the extremely low thermal conductivity of air in closed pores, which contributes to a lower thermal conductivity value [56].

Geopolymers incorporating different types of Spanish calcined clays and biomass bottom ash have a higher bulk density (Table 6) and higher values of thermal conductivity (Fig. 5) than control geopolymers. The thermal conductivity values are similar due to the geopolymers have a similar porosity. The decrease in thermal conductivity follows the following order GMK-BBA-YC ~ GMK-BBA-WC > GMK-BBA-BC > GMK-BBA-RC, with thermal conductivity values in the range 0.24–0.27 W/mK. It can be seen that the increase in the Si/Al ratio in geopolymers produced an increase in thermal conductivity. These results are in agreement with those found by Kamseu et al. [55,57], who demonstrated that the pore size of metakaolin-based geopolymers varies with the Si/Al ratio. These authors found that the thermal conductivity of metakaolin-based geopolymers increases linearly from 0.28 W/mK for geopolymers with a Si/Al = 1.3 M ratio up to 0.35 W/mK for geopolymers with a Si/Al = 2.5 M ratio. The results obtained in this study are comparable to those obtained by Villaquiran-Caicedo et al. [58]. These authors prepared geopolymers with thermal conductivities between 0.17 and 0.35 W/m K for metakaolin-based geopolymers using rice husk silica and silica fume as a source of silica. In general, the geopolymers obtained in this investigation have a low thermal conductivity (<0.30 W/mK) due to the fact that the geopolymerization reaction gives rise to polyoxalates of amorphous structure and intercon-

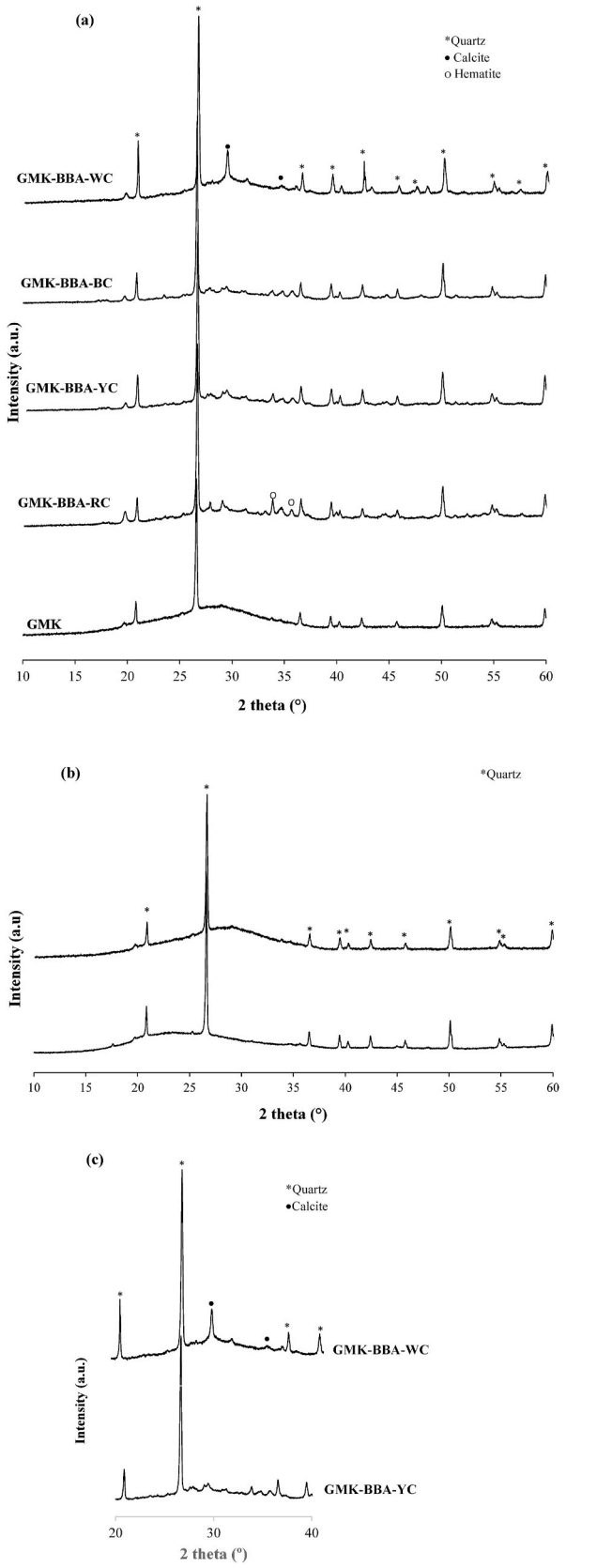

Fig. 7. XRD patterns of (a) geopolymers after 28 days; (b) control geopolymers (GMK) and MK precursor; (c) GMK-BBA-YC and GMK-BBA-WC geopolymers.

nected pores that provide a tortuous route for the flow of thermal gradient [59,60]. The amorphous structure of the geopolymer restricts heat transfer.

Furthermore, the thermal conductivity values obtained for the geopolymers developed in this study are similar to those of other materials used in thermal insulation such as Portland cement with a thermal conductivity of approximately 0.29 W/mK, or light concrete with a thermal conductivity of 0.23 W/mK [61].

3.5. X-ray diffraction (XRD) of geopolymers

Fig. 7a shows the X-ray diffraction diagrams of different geopolymers manufactured after 28 days of curing. In the control geopolymers (GMK) it can be seen that the quartz crystalline phase present in the MK raw material is also present. In the rest of geopolymers that incorporate BBA and different calcined clays, in addition to the diffraction peaks corresponding to MK, diffraction peaks corresponding to BBA precursors and calcined clays, such as calcium carbonate and hematite, are observed. This last phase is present in geopolymers using red clay as raw material (GMK-BBA-RC). The crystalline phases are mainly the non-reactive phases in the geopolymerization reaction. However, in all geopolymers the observed diffraction peaks are less intense than in the raw materials. These phases therefore appear as non-reactive particles and act as filler particles in the geopolymeric paste [52,62]. No new crystalline phases appeared in the geopolymerization process. The displacement observed in the halo of the precursor MK (15°-35°) after alkaline activation and subsequent geopolymerization (18°-38°) (Fig. 7b) is induced by alkali cations that promote the dissolution and subsequent destruction of the solid's silicoaluminate structure to give rise to aluminosilicate gel. Therefore, the microstructure of these materials is mainly constituted by an amorphous aluminosilicate phase generated where the halo observed in the 2θ range between 18° and 38° is a sign of the activity of the geopolymerization reaction, attributed to the aluminosilicate gel phase [63–66] and to the absence of a short-range order of metal oxides [67]. The replacement of BBA and different calcined clays causes the position of the amorphous halo to shift slightly to the right, indicating that with the incorporation of these raw materials, there are some changes in the geopolymeric gel formation [68]. This amorphous phase improves the mechanical properties of the geopolymeric matrix. The higher the amorphous phase content, the greater the mechanical strength of geopolymers [69]. This halo is slightly less intense in samples MK-BBA-YC (Fig. 7c) and MK-BBA-BC, indicating a lower amount of geopolymer gel in these specimens than in geopolymers using WC as raw material and RC, MK-BBA-WC (Fig. 7c) and MK-BBA-RC geopolymers, respectively, according to the compressive strength data.

3.6. FTIR observation of geopolymers

Fig. 8a shows the FTIR spectrum of the control geopolymers after 28 days, along with the FTIR spectrum of the MK precursor. The geopolimeryzation process of the aluminosilicate source can be verified by the disappearance or modification of some of the characteristic bands of the metakaolin (MK), particularly the one located at 1058 cm^{-1}. This band presents a shift towards lower frequencies (972 cm^{-1}) with the incorporation of the activating solution. This displacement is associated with the dissolution of the aluminosilicate source, due to the geopolymerization reaction of the silicate group with the formation of the geopolymeric gel, which is an evidence that the process of geopolymerisation has taken place. The width of the band centered at 972 cm^{-1} may be due to the superposition of different types of vibrational bands related to the T – O bond, where T can be Si or Al, that is, Al–O–Si, Si–O–Al, or Si–O–M (M: Na) [70]. The displacement observed in FTIR agrees with the displacement observed in the amorphous halo in the XRD difractograms. Another band that disappears in the geopolymeric material is that located at 796 cm^{-1}, attributed to the AlO_4 species of the metakaolin.

The substitution of MK for 33.33% of BBA and the additional substitution of another 33.33% of MK for different types of natural calcined clays, YC, RC, WC and BC after 28 days (Fig. 8b–e) show differences with respect to the FTIR spectra of the precursors used. In the FTIR spectra of biomass bottom ash and of the different types of calcined clays, a band centered at 987 cm^{-1} in the residue and between 990 and 984 cm^{-1} in the different types of calcined clays is observed. This band could be assigned to the stretching modes of the Si–O bond present in raw materials. In all geopolymers, a displacement of this band can be observed towards smaller wavenumbers (970-975 cm^{-1}), indicating the formation of the geopolymeric gel. The width of this band is primarily assigned to the short-range ordering of the Si and Al tetrahedra, as well as to the amorphous nature of the material. Fig. 9 shows the FTIR spectrum of all geopolymers cured at 28 days. In all geopolymers, the addition to the band observed at 970-975 cm^{-1} which is the fingerprint of the geopolymerization process, a wide band centered at 3368-3449 cm^{-1}, attributed to the tension vibration of the –OH bond of the free or physically absorbed water in the pores or surface of the gel can be observed. A second band centered at approximately 1643–1647 cm^{-1}, corresponding to the deformation vibration of the H–OH bond, can also be distinguished [71]. The bands located around, 2360 and 1450-1430 cm^{-1} can be attributed to asymmetric tension vibrations of the C–O bond of carbonates present in the geopolymer. These are complemented by a band located approximately at 870 cm^{-1} that corresponds to the symmetrical deformation vibration of the O–C–O bond [72,73]. The presence of carbonates is possibly due of unreacted $CaCO_3$ from the raw materials (Table 5) or to the interaction of the surface material with the CO_2 in the environment to form sodium and/or calcium carbonates. The bands located in the region between 600 cm^{-1} and 800 cm^{-1} are related to the Al–O bond tension vibrations, specifically for Al ions with coordination 4. The bands located in the region between 400 and 600 cm^{-1} can be associated with vibrations due to deformation of the bond Si–O–Si and Al–O–Si. Therefore, the bands located between 500 and 800 cm^{-1} are called SBU type vibration bands “Secondary Building Units”, and their position depends on the organizational form of the SiO_4 and AlO_4 tetrahedra, either in single or double rings and which can possess between 4, 5 or 6 units per ring [74].

Fig. 10 shows the influence of the age on the geopolymerization reaction of the GMK-BBA-WC geopolymers. A decrease in the bands centered at approximately 1650 and 3400 cm^{-1} can be obseverd indicating a water consumption during the progress of the geopolymerization reaction with the age. This fact is corroborated by the displacement of the band centered at approximately 955 cm^{-1} (Fig. 10) towards higher wavenumbers as the storage time increases (970 cm^{-1}), indicating an advance in the geopolymerization reaction with the formation of the geopolymeric gel responsible for hardening the material, as occurs in other similar geopolymeric systems [43,70]. However, after 7 days, there are hardly any differences in the FTIR spectra, indicating that for this age, the geopolymerization reactions have practically completed.

3.7. SEM-EDS analysis of geopolymers

SEM images were made to the geopolymers after 28 days to observe the microstructure (Fig. 11). The effects of the geopolymerization process, the formation of the geopolymer gel, due to the presence of the alkaline activator sodium hydroxide (NaOH) and sodium silicate (Na_2SiO_3) can be observed in all samples. In the GMK control geopolymers, the formation of the hydrated sodium aluminosilicate gel (Na-A-S-H) is observed. The addition of BBA and different types of Spanish calcined clays gives rise to geopolymers with a higher degree of densification, obtaining a denser structure in the GMK-BBA-WC and GMK-BBA-RC geopolymers. The incorporation of the residue and the different

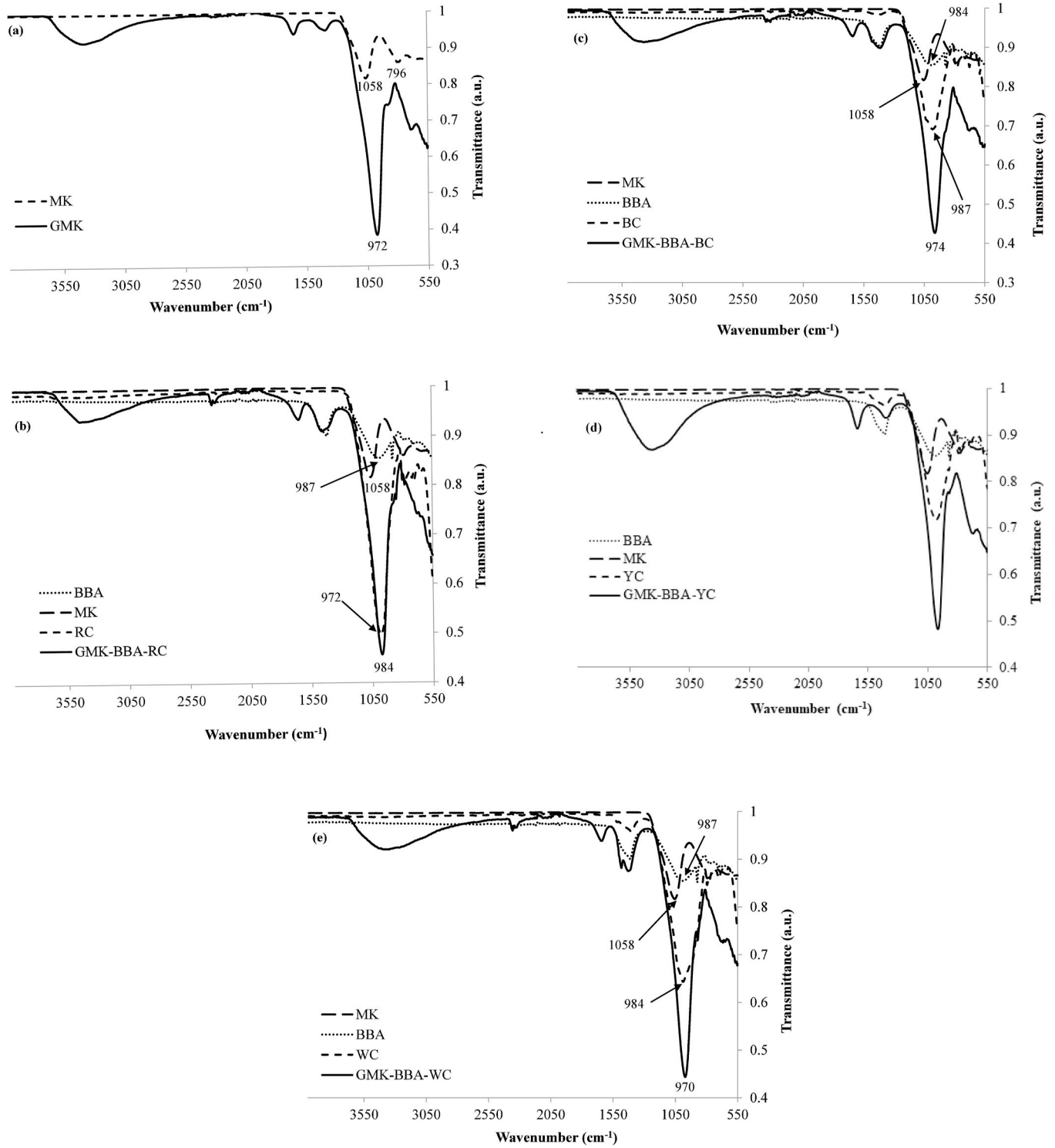

Fig. 8. FTIR spectra of (a) control geopolymers (GMK) and MK precursor; (b) GMK-BBA-YC; (c) GMK-BBA-RC (d) GMK-BBA-BC and (e) GMK-BBA-WC and precursors after 28 days.

types of clay gives rise to the generation of another type of geopolymeric gel richer in Ca (Ca-A-S-H or Ca–Na–S–H) gel, as well as the presence of unreacted clay platelets and dispersed unreacted bottom ash that surround the gel or binder phase. It suggests an insufficient dissolution of some components present in BBA and calcined clays that are not involved in the geopolymerization reaction. In the GMK-BBA-YC and GMK-BBA-BC geopolymers, a greater number of unreacted particles can be observed, indicating a lower degree of dissolution of the YC and BC samplesaccording to the results obtained in the HCl extraction (Table 5). This lower degree of bonding and less compact microstructure agrees well with the lower values of compressive strength. Also in geopolymers the existence of significant porosity is observed. This porosity has also been reported by other authors [75,76]. This porosity is higher in the control samples, as well as in the GMK-BBA-YC and GMK-BBA-BC geopolymers, observing the existence of a higher proportion of cracks due to the drying contraction of the reaction products [77]. These cracks can lead to a decrease in mechanical strength, as indicated by compressive strength data.

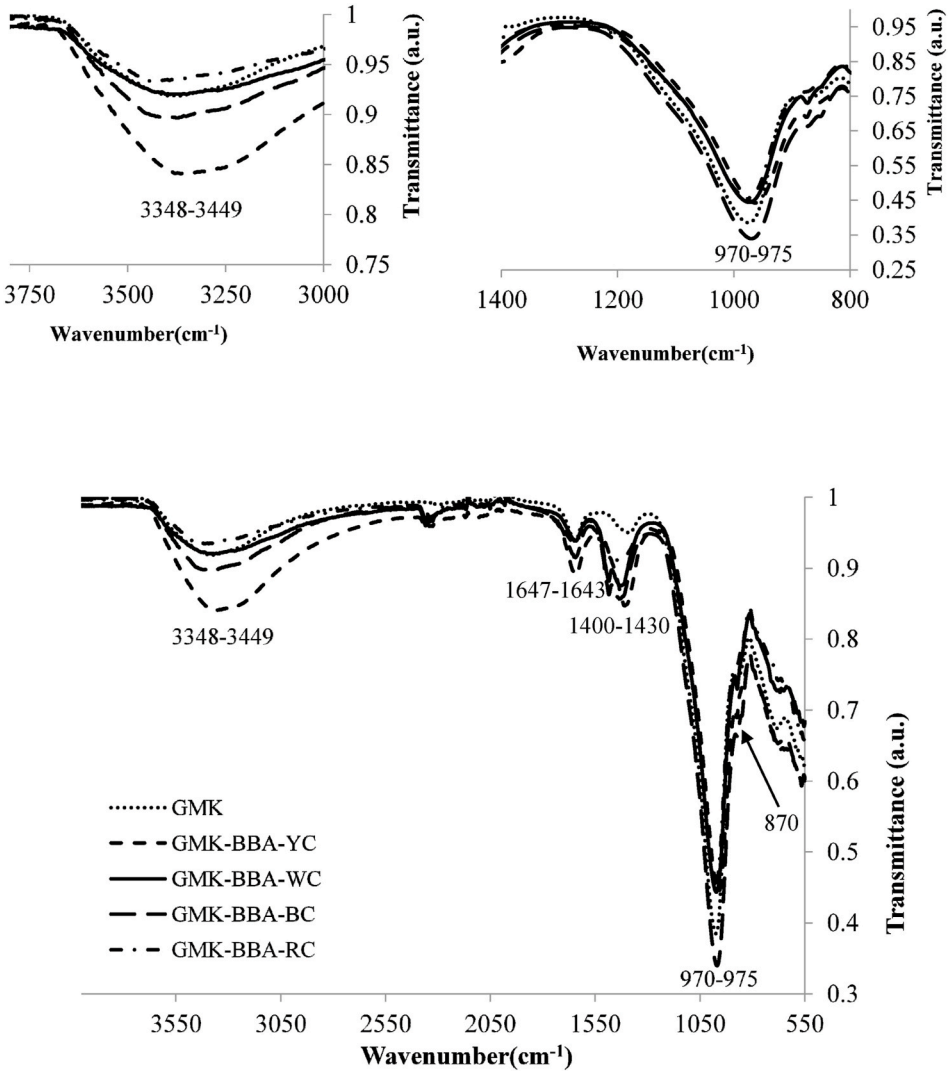

Fig. 9. FTIR spectra of geopolymers after 28 days.

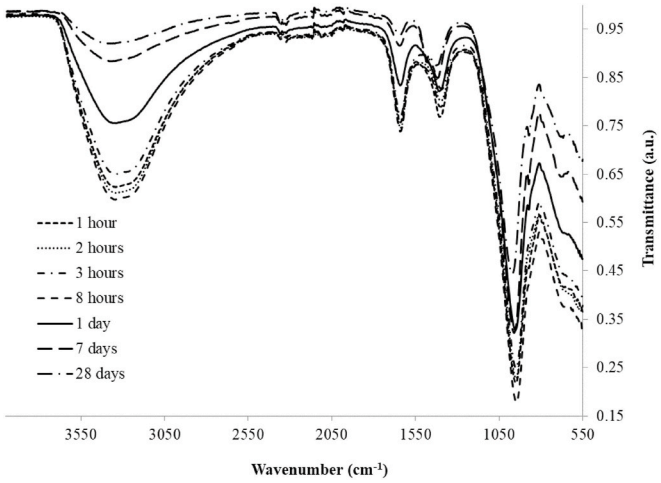

Fig. 10. FTIR spectra of GMK-BBA-WC geopolymers as function of time.

Table 7 shows the EDS analysis of each sample. The chemical compositions of geopolymers mainly include silicon (Si), aluminum (Al), sodium (Na) and calcium (Ca). Also, other elements such as potassium (K), iron (Fe) and magnesium (Mg) are observed, not included in Table 6, as they are found in a lower proportion. High amounts of Si, Al, Na and Ca provided the suitable conditions for the formation of the sodium silicate gel in the control geopolymers (GMK) and the hydrated sodium-calcium aluminosilicate gel (Na–C-A-SH) in the rest of geopolymers. It can be seen how the substitution of MK by BBA and different types of calcined clays gives rise to geopolymers with a higher Si/Al ratio, obtaining the highest values for the G-MK-BBA-RC and G-MK-BBA-WC geopolymers. The Si/Al ratio is important in the behavior of geopolymeric products [78]. A high Si/Al ratio indicates a geopolymer with a high compressive strength, while a low Si/Na ratio indicates a high reaction speed [79]. The GMK-BBA-WC presented higher values of compressive strength than the rest of the geopolymers (Fig. 5), presenting the highest Si/Al ratio. Therefore, a high Si/Al ratio and a lower Si/Na ratio may indicate a higher degree of reaction of the dissolved raw materials [80] according to the results obtained by the HCl extraction.

4. Conclusions

The objective of this study was focused on evaluating alternative raw materials such as olive-pine biomass bottom ash and calcined clays (yellow, red, white or black) traditionally used in the brick and ceramic tile sector in southern Spain, can be succesfully used as a partial substitution for metakaolin in the manufacture of geopolymers.

The main conclusions of this investigation are depicted as follows:

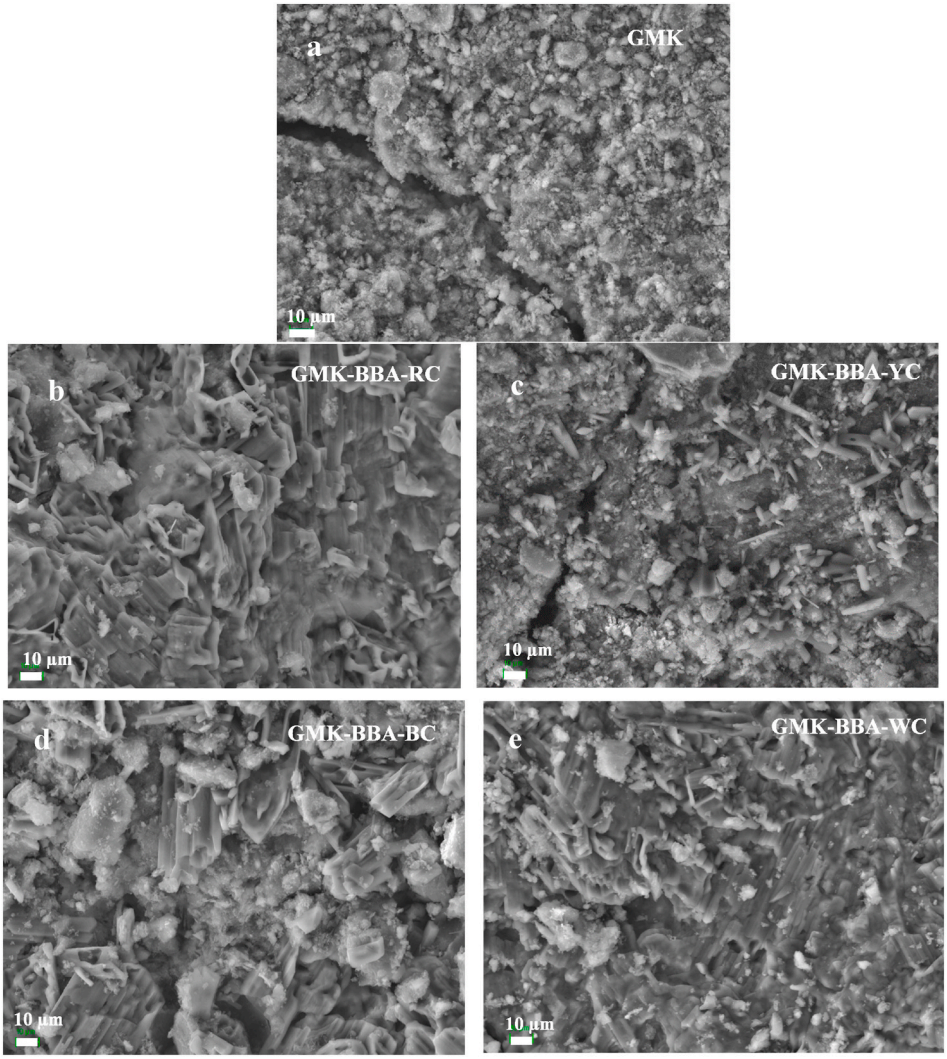

Fig. 11. SEM images of geopolymers: a) control geopolymers (MK) and geopolymers formulated with BBA and one of four different calcined clays, b) GMK-BBA-RC, c) GMK-BBA-YC, d) GMK-BBA-BC, and e) GMK-BBA-WC.

Table 7
SEM-EDS microanalysis of geopolymers.

Samples	Weight percentages (wt. %)				Ratio (wt. %)		
	Si	Al	Na	Ca	Si/Al	Si/Na	Si/Ca
GMK	31.70	18.67	8.32	–	1.70	3.84	–
GMK-BBA-RC	23.37	8.47	11.65	5.60	2.76	2.00	4.17
GMK-BBA-YC	24.03	10.15	10.20	6.84	2.37	2.36	3.51
GMK-BBA-BC	27.59	10.45	9.34	6.95	2.64	2.95	3.97
GMK-BBA-WC	17.50	5.74	21.51	5.72	3.06	0.84	3.05

- The mechanical strength achieved by geopolymers incorporating BBA and calcined clays is higher than that of control geopolymers prepared using MK. The increase in compressive strength may be due to the presence of minerals in the calcined clays that act as fillers, that is, to a filling effect exerted by the unreacted particles and/or the formation of some zones of C-A-S-H that coexist with N-A-S-H, due to the presence of calcium in the substitute raw materials. The maximum compressive strength is reached for geopolymers that use WC as raw material (GMK-BBA-WC), which can be explained due to an increase in the Si/Al ratio combined with a greater formation of C-(A)-S-H gel together with N-A-S-H gel and a lower presence of defects, such as micropores and microcracks.
- The thermal conductivity of the geopolymers that incorporate BBA and calcined clays increased slightly with respect to that of the control geopolymers (0.23 W/mK), increasing as the Si/Al molar ratio increases. However, the thermal conductivity values are low, presenting values between 0.27 and 0.24 W/mK similar to other construction materials.

These promising findings suggest that BBA, currently deposited in landfills, and the different types of clays currently used in traditional ceramics, can be used as raw materials in a new market within the geopolymer sector in the construction field, with economic and environmental benefits.

Author contribution

D. Eliche-Quesada performs some test, conceptualization.; data curation; supervision; funding acquisition and writing - original draft. A. Calero-Rodríguez, manufactures the geopolymer and performs some test. E. Bonet-Martinez performs some test. L. Pérez-Villarejo writing - review & editing. P.J. Sánchez-Soto writing - review & editing.

Declaration of competing interest

The authors declare that they have no known competing financial interests or personal relationships that could have appeared to influence the work reported in this paper.

Acknowledgments

This work has been funded by the project « Development and characterization of new geopolymer composites based on waste from the olive industry. Towards a sustainable construction (MAT2017-88097-R) », FEDER/Ministry of Science, Innovation and Universities, State Research Agency. The authors thank "Caobar S.A.", "Arcillas Bailén, S.L." and "Aldebarán Energía del Guadalquivir S.A." companies for supplying the kaolin, clays and biomass bottom ash, respectively. Technical and human support provided by CICT of Universidad de Jaén (UJA, MINECO, Junta de Andalucía, FEDER) are gratefully acknowledged.

References

[1] M.S. Imbabi, C. Carrigan, S. McKenna, Trends and developments in green cement and concrete technology, Int. J. Sustain. Built. Env. 1 (2012) 194–216, https://doi.org/10.1016/j.ijsbe.2013.05.001.
[2] J. Davidovits, Geopolymer chemistry and applications, Geopolymer Institute, fourth ed., Saint-Quentin, France, 2015, pp. 1–585.
[3] M.W. Grutzeck, D.D. Siemer, Zeolites synthesized from class F fly ash and sodium aluminate slurry, J. Am. Ceram. Soc. 80 (1997) 2449–2458, https://doi.org/10.1111/j.1151-2916.1997.tb03143.x.
[4] N.C. Nasvi, P.G. Ranjith, J. Sanjayan, The permeability of geopolymer at down-hole stress condition: aplication for carbon dioxide sequestration wells, Appl. Energy 102 (2013) 1391–1398, https://doi.org/10.1016/j.apenergy.2012.09.004.
[5] L. Miqueleiz, F. Ramírez, A. Seco, R.M. Nidzam, J.M. Kinuthia, A. AbuTair, R. García, The use of stabilised Spanish clay soil for sustainable construction materials, Eng. Geol. 133–134 (2012) 9–15, https://doi.org/10.1016/j.enggeo.2012.02.010.
[6] A.A. Shubbar, M. Sadique, P. Kot, W. Atherton, Future of clay-based construction materials – a review, Construct. Build. Mater. 210 (2019) 391–412, https://doi.org/10.1016/j.conbuildmat.2019.03.104.
[7] C. Aramburo, C. Pedrajas, V. Rahhal, M. González, R. Talero, Calcined clays for low carbon cement: rheological behaviour in fresh Portland cement pastes, Mater. Lett. 239 (2019) 24–28, https://doi.org/10.1016/j.matlet.2018.12.050.
[8] J.A. Rodríguez-Liébana, A. López-Galindo, C. Jiménez de Cisneros, A. Gálvez, M. Rozalén, R. Sánchez-Espejo, E. Caballero, A. Peña, Adsorption/desorption of fungicides in natural clays from Southeastern Spain, Appl. Clay Sci. 132–133 (2016) 402–411, https://doi.org/10.1016/j.clay.2016.07.006.
[9] F. Franco, J.A. Cecilia, M. Pozo, L. Pardo, E. Bellido, C. García-Sancho, Microwave assisted acid treatment of kerolitic clays from the Neogene Madrid Basin (Spain) and its use in CO_2 capture processes, Microporous Mesoporous Mater. 292 (2020) 109749, https://doi.org/10.1016/j.micromeso.2019.109749.
[10] M.I. Carretero, M. Pozo, J.L. Legido, M.V. Fernández-González, R. Delgado, I. Gómez, F. Armijo, F. Maravere, Assessment of three Spanish clays for their use in pelotherapy, Appl. Clay Sci. 99 (2014) 131–143, https://doi.org/10.1016/j.clay.2014.06.022.
[11] F. Messina, C. Ferone, A. Molino, G. Roviello, F. Colangelo, B. Molino, R. Cioffi, Synergistic recycling of calcined clayey sediments and water potabilization sludge as geopolymer precursors: upscaling from binders to precast paving cement-free bricks, Construct. Build. Mater. 133 (2017) 14–26, https://doi.org/10.1016/j.conbuildmat.2016.12.039.
[12] C. Ferone, B. Liguori, I. Capasso, F. Colangelo, R. Cioffi, E. Cappelletto, R. Di Maggio, Thermally treated clay sediments as geopolymer source material, Appl. Clay Sci. 107 (2015) 195–204, https://doi.org/10.1016/j.clay.2015.01.027.
[13] B. Molino, A. De Vincenzo, C. Ferone, F. Messina, F. Colangelo, R. Cioffi, Recycling of clay sediments for geopolymer binder production. a new perspective for reservoir management in the framework of Italian legislation: the occhito reservoir case study, Materials 7 (8) (2014) 5603–5616, https://doi.org/10.3390/ma7085603.
[14] H. Mohsen, N.Y. Mostafa, Investigating the possibility of utilizing low kaolinitic clays in production of geopolymer bricks, Ceram.- Silik. 54 (2) (2010) 160–168.
[15] L. Yun-Ming, C.-Y. Heah, A.B. Mohd Mustafa, H. Kamarudin, Structure and properties of clay-based geopolymer cements: a review, Prog. Mater. Sci. 83 (2016) 595–629, https://doi.org/10.1016/j.pmatsci.2016.08.002.
[16] C. Ferone, B. Liguori, I. Capasso, F. Colangelo, R. Cioffi, E. Cappelletto, R. Di Maggio, Thermally treated clay sediments as geopolymer source material, Appl. Clay Sci. 107 (2015) 195–204, https://doi.org/10.1016/j.clay.2015.01.027.
[17] H. Xu, J.S.J. Van Deventer, Geopolymerisation of multiple minerals, Miner. Eng. 15 (2002) 1131–1139, https://doi.org/10.1016/S0892-6875(02)00255-8.
[18] Directive 2009/28/EC of the European Parliament and of the Council of 23 April on the promotion of the use of energy from renewable sources, Official Journal of the European Union 140 (2009) 16–62.
[19] Informe de Infraestructuras energéticas de Andalucía, Agencia Andaluza de la Energía, Consejería de Hacienda, Industria y Energía, Actualizado a 31 de Diciembre de 2019) https://www.agenciaandaluzadelaenergia.es/sites/default/files/documentos/informe_andaluz_miea_2019_12_31.pdf..
[20] A. Demeyer, J.C. Voundi Nkana, M.G. Verloo, Characteristics of wood ash and influence on soil properties and nutrient uptake: an overview, Bioresour. Technol. 77 (2001) 287–295, https://doi.org/10.1016/S0960-8524(00)00043-2.
[21] N.C. Cruz, F.C. Silva, L.A.C. Tarelho, S.M. Rodrigues, Critical review of key variables affecting potential recycling applications of ash produced at large-scale biomass combustion plants, Resour. Conserv. Recycl. 150 (2019) 104427, https://doi.org/10.1016/j.resconrec.2019.104427.
[22] N. Toniolo, A.R. Boccaccini, Fly ash-based geopolymers containing added silicate waste. A review, Ceram. Int. 43 (2017) 14545–14551, https://doi.org/10.1016/j.ceramint.2017.07.221.
[23] C. Leiva, M. Rodriguez-Galán, C. Arenas, B. Alonso-Fariñas, B. Peceño, A mechanical, leaching and radiological assessment of fired bricks with a high content of fly ash, Ceram. Int. 44 (11) (2018) 13313–13319, https://doi.org/10.1016/j.ceramint.2018.04.162.
[24] CEDEX, Centro de Estudios y Experimentación de Obras Públicas, Ashes from biomass incineration – technical report (in Spanish) 2019. http://www.cedexmateriales.es/catalogo-de-residuos/23/cenizas-procedentes-de-la-incineracion-de-biomasa/3/volumen-y-distribucion.html. (Accessed 13 September 2020).
[25] E. Bonet-Martínez, P. García-Cobo, L. Pérez-Villarejo, E. Castro, D. Eliche-Quesada, Effect of olive-pine bottom ash on properties of geopolymers based on metakaolin, Materials 13 (2020) 901, https://doi.org/10.3390/ma13040901.
[26] M. Vázquez, J. Jiménez- Millán, Clay raw materials of the Triassic Red Beds (Northen Jaén, Spain) for making ceramic construction materials, Mater. Construcción 273 (2004) 5–20.
[27] A.H. De Aza, X. Turrillas, M.A. Rodriguez, T. Duran, P. Peña, Time-resolved powder neutron diffraction study of the phase transformation sequence of kaolinite to mullite, J. Eur. Ceram. Soc. 34 (2014) 1409–1421, https://doi.org/10.1016/j.jeurceramsoc.2013.10.034.
[28] M.T. Cotes-Palomino, C. Martínez-García, D. Eliche-Quesada, L. Pérez-Villarejo, Production of ceramic material using wastes from brewing industry, Key Eng. Mater. 663 (2016) 94–104, https://doi.org/10.4028/www.scientific.net/KEM.663.94.
[29] A. Fernández-Jiménez, M. Monzo, M. Vicent, A. Barba, A. Palomo, Alkaline activation of metakaolin–fly ash mixtures: obtain of zeoceramics and zeocements, Microporous Mesoporous Mater. 108 (1–3) (2009) 41–49, https://doi.org/10.1016/j.micromeso.2007.03.024.
[30] N. Granizo, A. Palomo, A. Fernandez-Jiménez, Effect of temperature and alkaline concentration on metakaolin leaching kinetics, Ceram. Int. 40 (7) (2014) 8975–8985, https://doi.org/10.1016/j.ceramint.2014.02.071.
[31] D. Eliche-Quesada, E. Bonet-Martínez, L. Pérez-Villarejo, E. Castro, P.J. Sánchez-Soto, Effects of an illite clay substitution on geopolymer synthesis as an alternative to metakaolin, J. Mater. Civ. Eng. 33 (5) (2021) 04021072, https://doi.org/10.1061/(ASCE)MT.1943-5533.0003690.
[32] S.M. Ohlberg, D.W. Strickeler, Determination of percent crystallinity of partial devitrified glass by X-ray difraction, J. Am. Ceram. Soc. 45 (1962) 170–171.
[33] G. Kakali, T.H. Perraki, S. Tsivilis, E. Badogiannis, Thermal treatment of kaolin: the effect of mineralogy on the pozzolanic activity, Appl. Clay Sci. 20 (1–2) (2001) 73–80, https://doi.org/10.1016/S0169-1317(01)00040-0.
[34] UNE 403-200-93: Determination of Carbonate Content in Soils, 1993.
[35] A. Fernández-Jiménez, A. Palomo, Mid-infrared spectroscopic studies of alkali activated fly ash structure, Microporous Mesoporous Mater. 86 (2005) 207–214, https://doi.org/10.1016/j.micromeso.2005.05.057.
[36] UNE-EN 1015-10:2000/A1:2007, Methods of Test for Mortar for Masonry - Part 10: Determination of Dry Bulk Density of Hardened Mortar, 2000.
[37] UNE-EN 772-1:2011, Methods of Test for Masonry Units - Part 1: Determination of Compressive Strength, 2011.
[38] ISO 8302:1991, Thermal Insulation — Determination of Steady-State Thermal Resistance and Related Properties — Guarded Hot Plate Apparatus, 1991.
[39] W. Zhu, X. Chen, L.J. Struble, E.H. Yang, Characterization of calcium containing phases in alkali-activated municipal solid waste incineration bottom ash binder through chemical extraction and deconvoluted Fourier transform infrared spectra, J. Clean. Prod. 192 (2018) 782–789, https://doi.org/10.1016/j.jclepro.2018.05.049.
[40] S. Puligilla, P. Mondal, Co-existence of aluminosilicate and calcium silicate gel characterized through selective dissolution and FTIR spectral subtraction, Cement Concr. Res. 70 (2015) 39–49, https://doi.org/10.1016/j.cemconres.2015.01.006.
[41] N.A. Jaya, L. Yun-Ming, H. Cheng-Yong, M. Mustafa, A.B. Abdullah, K. Hussin, Correlation between pore structure, compressive strength and thermal conductivity of porous metakaolin geopolymer, Construct. Build. Mater. 247 (2020) 118641, https://doi.org/10.1016/j.conbuildmat.2020.118641.
[42] C. Tippayasam, P. Balyore, P. Thavorniti, E. Kamseu, C. Leonelli, P. Chindaprasirt, D. Chaysuwan, Potassium alkali concentration and heat treatment affected metakaolin-based geopolymer, Construct. Build. Mater. 104 (2016) 293–297, https://doi.org/10.1016/j.conbuildmat.2015.11.027.
[43] P. Duxson, G.C. Lukey, J.S.J. van Deventer, Thermal conductivity of metakaolin geopolymers used as a first approximation for determining gel interconnectivity, Ind. Eng. Chem. Res. 45 (2006) 7781–7788 J.S.J., https://doi.org/10.1021/ie060187.
[44] P. Rożek, M. Król, W. Mozgawa, Spectroscopic studies of fly ash-based geopolymers, Spectrochim. Acta Mol. Biomol. Spectrosc. 198 (2018) 283–289, https://doi.org/10.1016/j.saa.2018.03.034.
[45] A. Hakamy, F.U.A. Shaikh, I.M. Low, Thermal and mechanical properties of hemp fabric-reinforced nanoclay–cement nanocomposites, J. Mater. Sci. 49 (2014) 1684–1694, https://doi.org/10.1007/s10853-013-7853-0.
[46] M. Lizcano, A. Gonzalez, S. Basu, K. Lozano, M. Radovic, Effect of water content and

chemical composition on structural properties of alkaline activated metakaolin-based geopolymers, J. Am. Ceram. Soc. 95 (2012) 2169–2177, https://doi.org/10.1111/j.1551-2916.2012.05184.x.
[47] M.A. Longhi, E.D. Rodríguez, B. Walkley, Z. Zhang, A.P. Kirchheim, Metakaolin-based geopolymers: relation between formulation, physicochemical properties and efflorescence formation, Composites Part B 182 (2020) 107671, https://doi.org/10.1016/j.compositesb.2019.107671.
[48] C. Kuenzel, T.P. Neville, S. Donatello, L. Vandeperre, A.R. Boccaccini, C.R. Cheeseman, Influence of metakaolin characteristics on the mechanical properties of geopolymers, Appl. Clay Sci. 83–84 (2013) 308–314, https://doi.org/10.1016/j.clay.2013.08.023.
[49] A. Gharzouni, B. Samet, S. Baklouti, E. Joussein, S. Rossignol, Addition of low reactive clay into metakaolin-based geopolymer formulation: synthesis, existence domains and properties, Powder Technol. 288 (2016) 212–220, https://doi.org/10.1016/j.powtec.2015.11.012.
[50] I. Ozer, S. Soyer-Uzun, Relations between the structural characteristics and compressive strength in metakaolin based geopolymers with different molar Si/Al ratios, Ceram. Int. 41 (8) (2015) 10192–10198, https://doi.org/10.1016/j.ceramint.2015.04.125.
[51] E. Prud'homme, P. Michaud, E. Joussein, C. Peyratout, A. Smith, Rossignol, In situ inorganic foams prepared from various clays at low temperature, Appl. Clay Sci. 51 (2011) 15–22, https://doi.org/10.1016/j.clay.2010.10.016.
[52] A. Fernández-Jiménez, A. Palomo, Composition and microstructure of alkali activated fly ash binder: effect of the activator, Cement Concr. Res. 35 (2005) 1984–1992, https://doi.org/10.1016/j.cemconres.2005.03.003.
[53] L. Valentini, S. Contessi, M.C. Dalconi, F. Zorzi, E. Garbin, Alkali-activated calcined smectite clay blended with waste calcium carbonate as a low-carbon binder, J. Clean. Prod. 184 (2018) 41–49, https://doi.org/10.1016/j.jclepro.2018.02.249.
[54] K. Yip, G.C. Lukey, J.S.J. Van Deventer, The coexistence of geopolymeric gel and calcium silicate hydrate at the early stage of alkaline activation, Cement Concr. Res. 35 (2005) 1688–1697, https://doi.org/10.1016/j.cemconres.2004.10.042.
[55] E. Kamseu, B. Ceron, H. Tobias, E. Leonelli, M.C. Bignozzi, A. Muscio, A. Libbra, et al., Insulating behavior of metakaolin-based geopolymer materials assess with heat flux meter and laser flash techniques, J. Therm. Anal. Calorim. 108 (2012) 1189–1199.
[56] A. Wongsa, V. Sata, B. Nematollahi, J. Sanjayan, P. Chindaprasirt, Mechanical and thermal properties of lightweight geopolymer mortar incorporating crumb rubber, J. Clean. Prod. 195 (2018) 1069–1080, https://doi.org/10.1016/j.jclepro.2016.01.083.8.
[57] E. Kamseu, B. Nait-Ali, M.C. Bignozzi, C. Leonelli, S. Rossignol, D.S. Smith, Bulk composition and microstructure dependence of effective thermal conductivity of porous inorganic polymer cements, J. Eur. Ceram. Soc. 32 (2012) 1593–1603, https://doi.org/10.1016/j.jeurceramsoc.2011.12.030.
[58] M.A. Villaquiran-Caicedo, R. Mejíade Gutiérrez, S. Sulekar, C. Davis, J.C. Nino, Thermal properties of novel binary geopolymers based on metakaolin and alternative silica sources, Appl. Clay Sci. 118 (2015) 276–282, https://doi.org/10.1016/j.clay.2015.10.005.
[59] C. Kuenzel, L.M. Groverd, L. Vandeperre, A.R. Boccaccini, C.R. Cheeseman, Production of nepheline/quartz ceramics from geopolymer mortars, J. Eur. Ceram. Soc. 33 (2013) 251–258.
[60] P. He, D. Jia, S. Wang, Microstructure and integrity of leucite ceramic derived from potassium-based geopolymer precursor, J. Eur. Ceram. Soc. 33 (2013) 689–698.
[61] CTE, Catálogo de elementos constructivos. Código técnico de la edificación, España, Madrid, 2010.
[62] T. Alomayri, H. Assaedi, F.U.A. Shaikh, I.M. Low, Effect of water absorption on the mechanical properties of cotton fabric-reinforced geopolymer composites, J. Asian Ceram Soc. 30 (2014) 223–230, https://doi.org/10.1016/j.jascer.2014.05.005.
[63] A. Palomo, F.P. Glasser, Chemically-bonded cementitious materials based on metakaolin, Br. Ceram. Trans. J. 91 (4) (1992) 107–112.
[64] V.F. Barbosa, K.J.D. Mackenzie, Synthesis and characterization of materials inorganic polymers of alumina and silica: sodium polysialate polymers, Int. J. Inorg. Mater. 2 (4) (2000) 309–317, https://doi.org/10.1016/S1466-6049(00)00041-6.
[65] C. Chen, G. Habert, Y. Bouzidi, A. Jullien, Environmental impact of cement production: detail of the different processes and cement plant variability evaluation, J. Clean. Prod. 18 (5) (2010) 478–485.
[66] S.O. Sore, A. Messan, E. Prud'homme, G. Escadeillas, F. Tsobnang, Synthesis and characterization of geopolymer binders based on local materials from Burkina Faso – metakaolin and rice husk ash, Construct. Build. Mater. 124 (2016) 301–311.
[67] S. Yaseri, V. Masoomi Verki, M. Mahdikhani, Utilization of high volume cement kiln dust and rice husk ash in the production of sustainable geopolymer, J. Clean. Prod. 230 (2019) 592–602, https://doi.org/10.1016/j.jclepro.2019.05.056.
[68] S. Yang, A. Navrotsky, B.L. Phillips, In situ calorimetric, structural, and compositional study of zeolite synthesis in the system 5.15 Na_2O– 1.00 Al_2O_3 – 3.28 SiO_2 – 165 H_2O, J. Phys. Chem. B 104 (25) (2000) 6071-6080.60.
[69] H. Hamdane, Y. Tamraoui, S. Mansouri, M. Oumam, A. Bouih, T. El Ghailassi, R. Boulif, B. Manoun, H. Hannache, Effect of alkali-mixed content and thermally untreated phosphate sludge dosages on some properties of metakaolin based geopolymer material, Mater. Chem. Phys. 248 (2020) 122938, https://doi.org/10.1016/j.matchemphys.2020.122938.
[70] T. Bakharev, Thermal behaviour of geopolymers prepared using class F fly ash and elevated temperature curing, Cement Concr. Res. 36 (2006) 1134–1147, https://doi.org/10.1016/j.cemconres.2006.03.022.
[71] A. Hajimohammadi, T. Ngo, P. Mendis, A. Kashani, J.S. Van Deventer, Alkali activated slag foams: the effect of the alkali reaction on foam characteristics, J. Clean. Prod. 147 (2017) 330–339, https://doi.org/10.1016/j.jclepro.2017.01.134.
[72] M. Król, J. Minkiewicz, W. Mozgawa, IR spectroscopy studies of zeolites in geopolymeric materials derived from kaolinite, J. Mol. Struct. 1126 (2016) 200–206, https://doi.org/10.1016/j.molstruc.2016.02.027.
[73] D. Panias, I.P. Giannopoulou, T. Perraki, Effect of synthesis parameters on the mechanical properties of fly ash-based geopolymers, Colloids Surf. A Physicochem. Eng. Asp. 301 (2007) 246–254, https://doi.org/10.1016/j.colsurfa.2006.12.064.
[74] S. Lee, M.D. Seo, Y.J. Kim, H.-H. Parkm, T.-N. Kim, Y. Hwang, S.-B. Cho, Unburned carbon removal effect on compressive strength development in a honeycomb briquette ash-based geopolymer, Int. J. Miner. Process. 97 (1–4) (2010) 20–25, https://doi.org/10.1016/j.minpro.2010.07.007.
[75] S. Selmani, A. Sdiri, S. Bouaziz, E. Joussein, S. Rossigno, Effects of metakaolin addition on geopolymer prepared from natural kaolinitic clay, Appl. Clay Sci. 146 (2017) 457–467, https://doi.org/10.1016/j.clay.2017.06.019.
[76] N. Koshy, K. Dondrob, L. Hu, Q. Wena, J.N. Meegoda, Synthesis and characterization of geopolymers derived from coal gangue, fly ash and red mud, Construct. Build. Mater. 206 (2019) 287–296, https://doi.org/10.1016/j.conbuildmat.2019.02.076.
[77] A.M. Rashad, D.M. Sadek, H.A. Hassan, An investigation on blast-furnace stag as fine aggregate in alkali-activated slag mortars subjected to elevated temperatures, J. Clean. Prod. 112 (2016) 1086–1096, https://doi.org/10.1016/j.jclepro.2015.07.127.
[78] J. He, Synthesis and Characterization of Geopolymers for Infrastructural Applications Ph.D. Thesis The Graduate Faculty of the Louisiana State University and Agricultural and Mechanical College, Baton Rouge, Louisiana, U.S, 2012.
[79] I.B. Topcu, M.U. Toprak, T. Uygunoglu, Durability and microstructure characteristics of alkali activated coal bottom ash geopolymer cement, J. Clean. Prod. 81 (2014) 211–217, https://doi.org/10.1016/j.jclepro.2014.06.037.
[80] A. Sathonsaowaphak, P. Chindaprasit, K. Pimraska, Workability and strength of lignite bottom ash geopolymer mortar, J. Hazard Mater. 168 (2009) 44–50, https://doi.org/10.1016/j.jhazmat.2009.01.120.